ISSN 0021-3640, JETP Letters, 2019, Vol. 110, No. 4, pp. 242–249. © Pleiades Publishing, Inc., 2019.
Russian Text © The Author(s), 2019, published in Pis'ma v Zhurnal Eksperimental'noi i Teoreticheskoi Fiziki, 2019, Vol. 110, No. 4, pp. 222–229.

FIELDS, PARTICLES, AND NUCLEI

Angular Distributions and Anisotropy of Fragments from the Neutron-Induced Fission of ^{237}Np in the Energy Range of 1–200 MeV: Measurement Data and Model Calculations

A. S. Vorobyev[a, *], A. M. Gagarski[a], O. A. Shcherbakov[a], L. A. Vaishnene[a], and A. L. Barabanov[b, c]

[a] *Petersburg Nuclear Physics Institute, National Research Center Kurchatov Institute, Gatchina, 188300 Russia*

[b] *National Research Center Kurchatov Institute, Moscow, 123182 Russia*

[c] *Moscow Institute of Physics and Technology (State University), Dolgoprudnyi, Moscow region, 141700 Russia*

**e-mail: vorobyev_as@pnpi.nrcki.ru*

Received June 17, 2019; revised July 8, 2019; accepted July 14, 2019

The experimental data on the angular distributions of fragments from the fission of ^{237}Np nuclei induced by 1–200 MeV neutrons have been presented. Such measurements for neutron energies above 16 MeV have been performed for the first time. These distributions have been analyzed and the angular anisotropy in the center-of-mass of fragments has been determined in the entire energy range under study. A method involvng the complex dynamics of the formation and decay of highly excited nuclei and based on the TALYS program has been proposed to calculate the angular distributions of fission fragments in a wide energy range for the collision of nuclei with neutrons. It has been shown that the developed model describes well the main features of the energy dependence of the angular anisotropy for the ^{237}Np target nuclei and can be used to extract new information on the reaction and fission process.

DOI: 10.1134/S0021364019160124

The measurement of angular distributions of neutron-induced fission fragments of nuclei at relatively low (below 20 MeV) and intermediate (below 200 MeV) energies is of interest for at least two reasons. First, the results of such measurements are important for improving model concepts of mechanisms of neutron-induced nuclear reactions, in particular, the fission reaction. Second, they are important for the development of new neutron technologies, including those associated with using accelerator-driven systems in the nuclear power industry, radiation tests of materials, and nuclear medicine. This work continues the series of our studies of angular distributions of neutron-induced fission fragments of nuclei with energies of 1–200 MeV reported in [1–5], where we presented experimental data obtained for ^{nat}Pb, ^{209}Bi, ^{232}Th, ^{233}U, ^{235}U, ^{238}U, and ^{239}Pu target nuclei. The measurements were performed at the Petersburg Nuclear Physics Institute, National Research Center Kurchatov Institute, with an intense neutron source based on a proton synchrocyclotron with a beam energy of 1 GeV on the 36-m flight base of the GNEIS time-of-flight spectrometer [6, 7]. Similar studies are also being performed currently at the n_TOF [8, 9] and LANSCE [10] facilities.

In this work, we present new measurement results for angular distributions of neutron-induced fission fragments of ^{237}Np nuclei, as well as our theoretical model allowing the calculation of these angular distributions. A model based on similar foundations was previously used in [11] to calculate the angular anisotropy of fragments from the fission of even–even nuclei ^{232}Th and ^{238}U induced by neutrons with energies of 2–100 MeV, but results for other nuclei were not reported. Furthermore, any detailed calculations in this field are absent.

The experimental setup and method of measurements of angular distributions of fission fragments were described in detail in our previous works cited above. We briefly describe only the main points. A target containing 99.99%-enriched ^{237}Np and being a NpO_2 layer about 300 μg/cm^2 in thickness and 80 mm in diameter on a 100-μm-thick aluminum backing 100 mm in diameter was fabricated by the standard "painting" method. Fission fragments were detected by two position-sensitive multiwire proportional counters placed on a beam one behind the other. The axis of the neutron beam was perpendicular to the plane of the position-sensitive multiwire proportional counters and passed through their geometrical centers. The data acquisition system was based on a 500 MHz FLASH analog-to-digital converter. Digital signal processing methods allowed the measurements of angular distributions of fission fragments in a wide

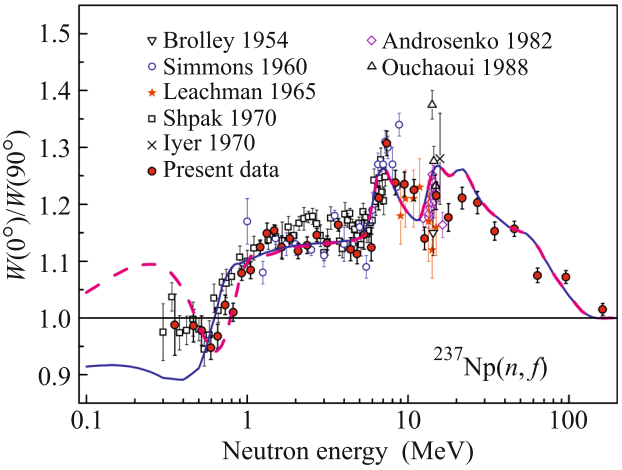

Fig. 1. (Color online) Angular anisotropy of fission fragments of ^{237}Np versus the incident neutron energy E along with the data from [12–18]. The solid and dashed lines are calculations in variants 1 and 2, respectively (see the main text).

energy range of neutrons inducing fission with almost zero threshold for fission fragment detection. In these measurements, we achieved an almost ideal separation of fission events from accompanying reactions (for details, see [2]). Corrections were introduced to the measured distributions to take into account the real geometry of the experiment, as well as the design and features of operation of the position-sensitive multiwire proportional counters. To obtain angular distributions in the center-of-mass system of fission fragments, we determined the effect of the momentum transferred by the incident neutron to the fissioning system on angular distributions in the laboratory system. To this end, angular distributions of fission fragments in the laboratory system were measured for two positions of successively located counters with respect to the incident neutron beam. In the first, downstream, position, the beam direction coincides with the longitudinal momentum component of the detected fission fragment. In the second, upstream, position, the beam direction is opposite to the longitudinal momentum component of the detected fission fragment (see [3]).

Let σ_f and $d\sigma_f(\theta)/d\Omega$ be the total and differential fission cross sections, where θ is the center-of-mass emission angle of the light (for definiteness) fission fragment with respect to the neutron beam axis (z axis). It is convenient to represent the angular distribution of fission fragments in the form of an expansion in even Legendre polynomials:

$$W(\theta) \equiv \frac{1}{\sigma_f}\frac{d\sigma_f(\theta)}{d\Omega} = \frac{1}{4\pi}\left(1 + \sum_{Q=2,4,\ldots} A_Q P_Q(\cos\theta)\right). \quad (1)$$

We measured the angular distributions of the fission fragment of ^{237}Np nuclei in the angular range of $0.24 < \cos(\theta) < 1.0$ with a step of $\cos(\theta) = 0.01$ for incident neutron energies in the range of 0.4–160 MeV. The angular distribution at each energy was approximated by Eq. (1); in all cases, it was sufficient to take into account the second and fourth Legendre polynomials. Figure 1 shows the anisotropy calculated with the found parameters A_2 and A_4 by the formula

$$\frac{W(0°)}{W(90°)} = \frac{1 + A_2 + A_4}{1 - A_2/2 + 3A_4/8}. \quad (2)$$

This figure also shows the results of seven preceding measurements of this anisotropy [12–18] included in the EXFOR database [19]. Below 16 MeV, our values are generally in agreement with the data of other groups within experimental errors. Some discrepancies are observed in the energy range of 2–5 MeV, where our results are close to the data from [13] but differ from the data reported in [16]. The angular anisotropy of neutron-induced fission fragments of ^{237}Np at energies above 16 MeV was measured for the first time. The average error of our measurements in the entire neutron energy range of 0.4–160 MeV is about 1–2%.

To describe data on the angular anisotropy, we developed a theoretical model for the calculation of the differential cross section for neutron-induced fission of nuclei at low and intermediate energies. The cross section below the threshold of the $(n,n'f)$ reaction is primarily due to the binary (n,f) reaction. However, the situation is successively complicated as the center-of-mass collision energy exceeds the threshold of the $(n,n'f)$, $(n,2nf)$, etc., reactions. To obtain the observed fission cross section, the fission cross sections of the second, third, etc., chances should be added to the binary fission cross section. In fact, complications begin earlier because the $(n,\gamma f)$, $(n,\ 2\gamma f)$, etc., reactions are zero-threshold. Let Z_0 and N_0 be the numbers of protons and neutrons in the primary compound nucleus, respectively, and Z and N be the corresponding numbers for the residual nucleus, which is formed and undergoes fission after a part of the excitation energy is spent on the emission of one or several particles. Let i enumerate the states of such residual nucleus with the spin J and parity π, $\sigma_{ZN}(J\pi;i)$ be the cross section for the population of the corresponding state, and $P_f^{ZN}(J\pi;i)$ be the probability of fission (fissionability) of this state. The observed fission cross section has the form

$$\sigma_f = \sum_{ZNJ\pi i} \sigma_{ZN}(J\pi;i) P_f^{ZN}(J\pi;i), \quad (3)$$

where summation over i becomes integration if states are in a continuous spectrum. The binary fission cross section is only a part of the cross section given by Eq. (3) and is determined by the terms corresponding to $Z = Z_0$, $N = N_0$, and $i = i_0$, where i_0 is the number

of the (J,π) compound state in the primary (Z_0, N_0) compound nucleus.

To describe the angular distributions of fission fragments, we used the concept by A. Bohr of transition nuclear states on the barrier, which are characterized by certain projections K of the spin J on the deformation axis (see, e.g., [20, 21]). The spatial part of the wavefunction of the nucleus in the transition state is proportional to $D^J_{MK}(\omega) = e^{iM\varphi}d^J_{MK}(\theta)e^{iK\psi}$, where M is the projection of the spin J on the z axis and $\omega = (\varphi, \theta, \psi)$ are the Euler angles specifying the orientation of the reference frame associated with the nucleus with respect to the immobile system (x, y, z). Since the deformation axis is transformed to the fission fragment emission axis, the normalized probability of emission $dw^J_{MK}(\theta)$ of the light fission fragment to the solid angle $d\Omega$ at the angle θ to the z direction is determined by the square of the absolute value of the wavefunction:

$$dw^J_{MK}(\theta) = \frac{2J+1}{4\pi}|d^J_{MK}(\theta)|^2 d\Omega. \quad (4)$$

In the general case, the spin orientation of the nucleus with respect to the z axis is specified by the nonuniform probability distribution $\eta^J(M)$ in the projection M and fission occurs through several transition states with different K values corresponding to a certain generally nonuniform probability distribution $\rho^J(K)$. Consequently, the angular distribution of fission fragments of the nucleus with the spin J and parity π has the form

$$\frac{dw^{J\pi}(\theta)}{d\Omega} = \sum_M \eta^{J\pi}(M)\sum_K \rho^{J\pi}(K)\frac{dw^J_{MK}(\theta)}{d\Omega}. \quad (5)$$

We represent the population cross section $\sigma_{ZN}(J\pi;i)$ appearing in Eq. (3) in the form of the sum of cross sections $\sigma_{ZN}(J\pi M;i)$ for population of states with the projection M of the spin J on the z axis. Then, the desired differential fission cross section is represented in the form

$$\frac{d\sigma_f(\theta)}{d\Omega} = \sum_{ZNJ\pi i}\sum_M \sigma_{ZN}(J\pi M;i)P_f^{ZN}(J\pi;i) \times \sum_{ZN}\sum_K \rho^{J\pi i}_{ZN}(K)\frac{dw^J_{MK}(\theta)}{d\Omega}. \quad (6)$$

In reactions involving particles whose spins are not oriented, the spin orientation of compound nuclei is due to the orbital angular momentum $\mathbf{l}$ of the incident particle, which is perpendicular to the z axis (collision axis). Since $\mathbf{J} = \mathbf{s} + \mathbf{I} + \mathbf{l}$, where $\mathbf{s}$ and $\mathbf{I}$ are the spins of the incident particle and target nucleus, respectively, the vector $\mathbf{J}$ in the semiclassical approximation predominantly has the direction perpendicular to the z axis. Therefore, the distribution $\eta^{J\pi}(M)$ in the projection M on the z axis for primary compound states is nonuniform. In this picture, $\eta^{J\pi}(M) = \eta^{J\pi}(-M)$; this type of the spin orientation is called alignment.

It is reasonable to expect that the nonuniformity of population of states in the quantum number M for secondary residual nuclei formed after the emission of a light particle by the compound nucleus decreases; i.e., the degree of alignment decreases. However, if the particle is emitted in a statistical process, its energy is about the temperature of the excited nucleus, i.e., relatively low. Consequently, the angular momentum carried by this particle is also low. For this reason, M distributions will be equated slowly. Correspondingly, fissioning nuclei formed even after a long statistical cascade of emitted particles can make a significant contribution to the anisotropy of the angular distribution of fission fragments. This circumstance for the fission of nuclei by intermediate energy neutron was confirmed for the first time in the calculation performed in [11].

Nonequilibrium processes should be taken into account at incident neutron energies exceeding 10–20 MeV. If ξ is the fraction of the reaction cross section σ_r corresponding to the cross section for the formation of an equilibrium compound nucleus, the remaining fraction $(1 - \xi)\sigma_r$ is due to cross sections for direct processes (such as knockout and pick-up) and processes of pre-equilibrium emission of particles. Such processes result in the formation of a residual nucleus usually in one of the excited states. In the continuous spectrum, the secondary equilibrium compound nucleus is generally formed with a certain probability ξ' and one of the light particles is emitted with the probability $1 - \xi'$ in the secondary pre-equilibrium process. Secondary and subsequent pre-equilibrium processes are referred to as multiple pre-equilibrium emission.

We make the usual assumption that fission occurs only from equilibrium compound states. In the general case, we separate the total fission cross section into two components. The component of the total fission cross section corresponding to the fission of the primary compound nucleus or residual nucleus formed at any stage of the statistical cascade decay of the primary compound nucleus is marked by the superscript C. The component corresponding to the fission of the residual nucleus formed after the emission of one or several particles, where the first particle is emitted in the direct or pre-equilibrium process, is marked by the superscript DPE. In the latter case, the first emitted particle usually has a high energy and, thereby, a high angular momentum. For this reason, even if the compound state of the secondary nucleus is formed immediately after the emission of this particle, the degree of its spin orientation will be low. Consequently, the angular distributions of fission fragments of such a

nucleus will be almost isotropic. The same is also true for the fission of any subsequent residual nucleus.

For simplicity, let all contributions to the differential fission cross section with the superscript DPE be isotropic; in this case, Eq. (6) is represented in the form

$$\frac{d\sigma_f(\theta)}{d\Omega} = \frac{\sigma_f^{DPE}}{4\pi} + \frac{d\sigma_f^C(\theta)}{d\Omega}, \quad (7)$$

$$\frac{d\sigma_f^C(\theta)}{d\Omega} = \sum_{ZNJ\pi i}\sum_M \sigma_{ZN}^C(J\pi M;i)P_f^{ZN}(J\pi;i) \times \sum_{ZN}\sum_K \rho_{ZN}^{J\pi i}(K)\frac{dw_{MK}^J(\theta)}{d\Omega}. \quad (8)$$

Here, $\sigma_{ZN}^C(J\pi M;i)$ is the cross section for the population of the (J,π,i) compound state of the (Z,N) nucleus with the spin projection M on the z axis either in the collision of a neutron with the target nucleus (in this case, $Z = Z_0$, $N = N_0$, and $i = i_0$) or (in all other cases) in a statistical cascade, which starts with the decay of one of the primary compound states. The observed angular distribution of fission fragments given by Eq. (1) is determined by the differential cross section (7) and total fission cross section $\sigma_f = \sigma_f^{DPE} + \sigma_f^C$.

If the excitation energy of the (J,π,i) state significantly exceeds the fission barrier, the statistical K distribution is used (see, e.g., [20]):

$$\rho_{ZN}^{J\pi i}(K) = \frac{e^{-K^2/2K_0^2}}{\sum_K e^{-K^2/2K_0^2}}, \quad (9)$$

where the parameter K_0^2 is determined by the temperature T of the nucleus on the barrier and the effective moment of inertia J_{eff},

$$K_0^2 = \frac{J_{eff}T}{\hbar^2}, \quad J_{eff} = \frac{J_\perp J_\parallel}{J_\perp - J_\parallel}. \quad (10)$$

Here, $J_\parallel$ and $J_\perp$ are the moments of inertia of the nucleus on the barrier with respect to the deformation axis and the axis that passes through the center of gravity of the nucleus and is perpendicular to the deformation axis. Distribution (9) is also often used at low excitation energies; in this case, the parameter K_0^2 is considered as fitting. A similar scheme was used in the calculation reported in [11]; in particular, the statistical distribution (9) was used for all nuclei at all excitation energies, a complex approximation was used for the energy dependence of K_0^2, and $K_0^2 = 2.5$ is accepted below a certain energy.

For calculations, we used the TALYS program (version 1.9) [22], which simulates a complex process of interaction of light particles with nuclei at energies up to 200 MeV (and even up to 1000 MeV in some cases) and calculates cross sections, in particular, the total fission cross section and other observables. The TALYS program also includes numerous characteristics of nuclei. The TALYS program allows the use of not only the parameters and models that are considered as optimal and, thereby, are specified by default, but also alternative parameters and models. Using the open code of the TALYS program, we modified it to expand the set of calculated parameters, in particular, the differential fission cross section, angular distributions of fission fragments, and the components σ_f^{DPE} and σ_f^C of the total fission cross section σ_f. The differential fission cross section (8) is determined primarily by the cross sections $\sigma_{ZN}^C(J\pi M;i)$ of the population of nuclear states, which depend on the projection M of the spin J on the z axis. In the existing version of the TALYS program, only the population cross sections $\sigma_{ZN}(J\pi;i)$ summed over M values are calculated; they can be decomposed into the DPE and C components, as the fission cross sections.

In fact, the knowledge of M dependences of all population cross sections is excessive. This can be easily understood if Eqs. (4) and (5) for the angular distribution are transformed to the form

$$\frac{dw^J(\theta)}{d\Omega} = \frac{1}{4\pi}\sum_{Q=0,2,4,\ldots}(2Q+1)\tau_{Q0}(J)\beta_Q(J)P_Q(\cos\theta). \quad (11)$$

Here, $\tau_{Q0}(J)$ are the irreducible components of the density matrix or, in other words, Qth rank orientation spin tensors (see, e.g., [23]) and $\beta_Q(J)$ are the Qth rank anisotropy parameters given by the formulas

$$\tau_{Q0}(J) = \sum_M C_{JMQ0}\eta^J(M), \quad \tau_{00}(J) = 1, \quad (12)$$

$$\beta_Q(J) = \sum_M C_{JKQ0}\rho^J(K), \quad \beta_0(J) = 1, \quad (13)$$

where C_{BbDd}^{Aa} is the Clebsch–Gordan coefficient. Summation in Eq. (11) is performed only over even Q values because $\beta_Q(J) = 0$ at odd Q values since $\rho^J = \rho^J(|K|)$ owing to the conservation of spatial parity. In addition, as shown above, at alignment, $\eta^J = \eta^J(|M|)$, so that $\tau_{Q0}(J) = 0$ at odd Q values in this case.

The spin tensors $\tau_{Q0}(J)$ decrease rapidly with increasing Q if the distribution $\eta^J(M)$ is smooth; the same is valid for quantities $\beta_Q(J)$ and distribution $\rho^J(K)$. Since at least one of the distributions $\eta^J(M)$ and $\rho^J(K)$ is almost always smooth in practice, the second and fourth Legendre polynomials are usually sufficient for the description of anisotropy (as already mentioned above in view of the processing of angular

distributions of neutron-induced fission fragments of ^{237}Np nuclei). Thus, to describe the angular distribution, it is sufficient to know only the spin tensors corresponding to the first several Q values. Correspondingly, using the TALYS program, we calculated not the M-dependent cross sections for the population of states but the orientation spin tensors of these states for $Q = 2,4,6$. In this approach, the C component of the differential fission cross section (8) has the form

$$\frac{\sigma_f^C(\theta)}{d\Omega} = \frac{1}{4\pi}\sum_{Q=0,2,4,\ldots}\sigma_{fQ}^C P_Q(\cos\theta), \qquad (14)$$

where $\sigma_{f0}^C \equiv \sigma_f^C$. The general expression (1) for the angular distribution of fission fragments with $A_Q = \sigma_{fQ}^C/\sigma_f$ follows from this formula.

To test this approach, we tried to reproduce the experimental data obtained for the ^{237}Np nucleus with the spin $I = 5/2$ and parity $\pi_0 = +1$ with the minimum possible number of excess parameters in addition to those used in the TALYS program (as a rule, we used the default parameters). However, the fission cross section in the $n + {}^{237}$Np reaction calculated with the usual explicit inclusion of the collective increase in the density of levels of fissioning nuclei and with the fission barriers and transition states from the RIPL-3 library [21] (incorporated in the TALYS program) differs from the measurement results reported in [24–26] almost in the entire range from 0.1 to 200 MeV (the discrepancy below 1 MeV is more than an order of magnitude—see Fig. 2). Above 20–30 MeV, the calculated cross section can be approached to the measured one by omitting multiple pre-equilibrium emission; for this reason, all our further calculations were performed omitting multiple pre-equilibrium emission. The range below 20–30 MeV was considered in detail in [26], where it was shown that the fission cross section calculated by the EMPIRE program (differing from the TALYS program in a number of parameters) with the parameters from the RIPL-3 library differs from the measured fission cross section, and a calculation with changed parameters of the barriers, transition states, and density of levels above the barriers that is in agreement with experimental data was presented. We do not aim at obtaining a similarly good description for the cross section, but perform some similar changes in the parameters of the transition states and barriers (retaining the parameters of the density of levels) for ^{238}Np, ^{237}Np, and ^{236}Np nuclei, whose inclusion is the most important in the range below 30 MeV (for simplicity, we omit the transition states for ^{237}Np and ^{236}Np). This allows us to obtain the fission cross section in the $n + {}^{237}$Np reaction, which is in reasonable agreement with the measured cross section up to 100 MeV (see Fig. 2), noticeably differing from it only in the ranges of 2–7 and 8–16 MeV, but by no more than 25–30% (we note that the considered problem

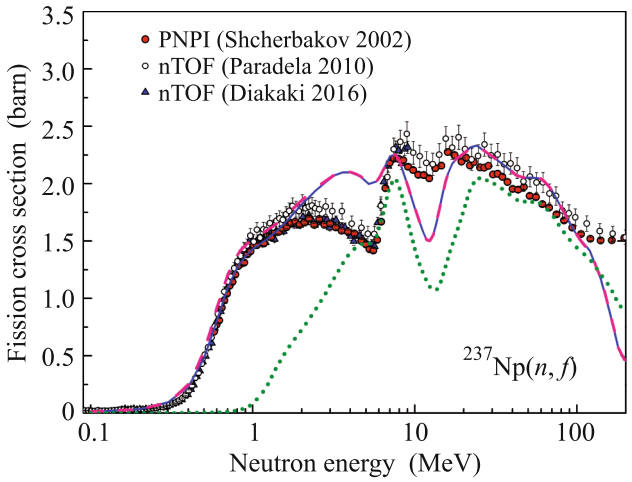

Fig. 2. (Color online) Fission cross section of ^{237}Np versus the incident neutron energy E: experimental data are taken from [24–26], the dotted line is the calculation with the parameters specified in the TALYS program by default, and the solid and dashed lines are the calculations in variants 1 and 2, respectively (see the main text).

does not have an unambiguous solution, so that we found only one of the possible sets of parameters). The range above 100 MeV will be discussed below. Table 1 presents the parameters of the fission barriers for the ^{238}Np, ^{237}Np, and ^{236}Np nuclei that we used to describe both the fission cross section and angular distribution of fission fragments. The fission cross section was calculated for two sets of transition states for ^{238}Np (variants 1 and 2 in Fig. 2), which will be discussed below.

Minimizing the number of the fitting parameters, we used the statistical distribution (9) and the parameter K_0^2 given by Eq. (10) down to the extremely low excitation energies E_{ex} of fissioning nuclei. The temperature of the nucleus on the barrier appearing in Eq. (10) is determined by the formula $T = \sqrt{U/a_{fi}(U)}$, where $U = E^* - \Delta$ is the effective excitation energy, $E^* = E_{ex} - B_{fi}$ is the excitation energy of the nucleus above the ith barrier, Δ is the parameter depending on Z and N and related to the nucleon pairing energy, and $a_{fi}(U)$ is the parameter of the density of levels depending on the energy and number i of the barrier; the

Table 1. Heights B_i (MeV) and widths $\hbar\omega_i$ (MeV) of the first and second fission barriers for ^{238}Np, ^{237}Np, and ^{236}Np nuclei used to describe the fission cross section and angular anisotropy of fission fragments in the $n + {}^{237}$Np reaction

Nucleus	B_1	$\hbar\omega_1$	B_2	$\hbar\omega_2$
^{238}Np	6.05	0.4	5.35	0.4
^{237}Np	5.4	1.0	5.2	0.5
^{236}Np	5.1	0.6	5.0	0.4

parameters B_{fi} (in addition to those presented in Table 1), Δ, and $a_{fi}(U)$ are specified in the TALYS program. Correspondingly, we assume that Eqs. (9) and (10) are valid at $E^* > \Delta + U_{up}$, where E^* is measured from the higher barrier and the energy U_{up} is the same for all nuclei. In this case, we determine U_{up} for the ^{238}Np nucleus as follows. The excitation energy of the compound nucleus is $E_{ex} = E_{cm} + B_n$, where E_{cm} is the center-of-mass collision energy between the neutron and ^{237}Np nucleus (which almost coincides with the neutron energy E in the laboratory system) and $B_n = 5.488$ MeV is the binding energy of the neutron in ^{238}Np. According to Fig. 1, the anisotropy varies very insignificantly in the range $E \simeq 1$–6 MeV or $E_{ex} \simeq 6.5$–11.5 MeV. Assuming that this indicates the validity of the statistical distribution in entire this range and taking into account that the lower bound of this range is approximately 0.4 MeV higher than the first, higher, barrier, we obtain $U_{up} = 0.4$ MeV because $\Delta = 0$ in the odd–odd ^{238}Np nucleus.

However, as the energy decreases below 1 MeV, the anisotropy decreases rapidly to values smaller than unity. This should be attributed to transition states. In a consistent approach, products $P_f^{ZN}(J\pi;i)\rho_{ZN}^{J\pi i}(K)$ in Eqs. (6) and (8) for this energy range would be replaced by the fissionabilities $P_f^{ZN}(J\pi K;i)$, which depend on K and are directly related to the transition states with the quantum numbers (J,π,K). However, such fissionabilities are not calculated in the TALYS program because this problem is insufficiently studied. In particular, modern presentations of methods for the description of fission for both fundamental and applied aims do not contain recommendations for calculations of fissionabilities as explicit (and significant) functions of K (see, e.g., [21]).

For this reason, at excitation energies comparable to the barrier height, we use the following approximation. Let fission at energies $E^* < \Delta + U_{down}$ occur primarily through the states with $|K|$ close to a certain value K_1 according to the formula

$$\rho_{ZN}^{J\pi i}(K) \sim e^{-\alpha(|K|-K_1)^2}. \quad (15)$$

Let the parameters U_{down} and α be identical for all nuclei, and the number K_1 can be chosen for each isotope, if necessary. For the K distribution in the range $\Delta + U_{down} < E^* < \Delta + U_{up}$, we take a function that is smoothly transformed with increasing E^* from Eq. (15) to Eq. (9). The values $U_{down} = -0.1$ MeV and $\alpha = 1.5$ are obtained from the reproduction of the angular anisotropy for $n + {}^{237}$Np at energies below 1 MeV. In this reproduction, K_1 is the key parameter. Varying it in the physically reasonable range from 0 to 4, we established that the observed angular anisotropy $W(0°)/W(90°) \simeq 0.95$ near $E = 0.5$ MeV (see Fig. 1) is reproduced only if the parameter K_1 is close to 0 or 4 (at all intermediate K_1 values, the angular anisotropy at this energy is either larger or very slightly smaller than unity). Here, the result is also sensitive to the transition states for the ^{238}Np nucleus, which are introduced to describe the fission cross section at low energies. In variant 1, we take $K_1 = 0$ and place states $(K,\pi) = (0,-)$, $(1,-)$, and $(3,-)$ in the 0.1 MeV interval above each barrier. In variant 2, we take $K_1 = 4$ and place states $(K,\pi) = (1,-)$, $(2,-)$, $(3,-)$, and $(4,-)$ in the same interval above each barrier. Both variants provide approximately the same description of the fission cross section (a very small difference is observed only in the range of 1–2 MeV—see Fig. 2).

Thus, our model for the calculation of the angular distribution of fragments from neutron-induced fission of nuclei at energies from very low, about 0.1 MeV, to intermediate, up to 200 MeV, based on the TALYS program contains the additional parameters α, U_{down}, U_{up}, and J_{eff} that are the same for all nuclei and the parameter K_1 that should be specified individually for each isotope. In practice, in addition to the above K_1 values for ^{238}Np, we accept $K_1 = 0.5$ for the ^{237}Np nucleus and $K_1 = 1.5$ for all other nuclei. The effective moment of inertia J_{eff} was chosen such that $\hbar^2/J_{eff} = 0.017$ MeV. The results of calculation of the angular anisotropy in the range from 0.1 to 200 MeV are shown in Fig. 1 for variants (solid line) 1 and (dashed line) 2. Above $E \simeq 1$ MeV or $E_{ex} \simeq B_{fi} + U_{up} \simeq 6.5$ MeV, where the K distribution in the ^{238}Np nucleus is statistical in both variants, the solid and dashed lines almost coincide with each other (differences in transition states in this nucleus are not manifested at these energies).

Our calculations confirm the conclusions made in [11] that nuclei fissioning at late stages of the reaction make a significant contribution to the observed angular anisotropy. For example, we consider a sufficiently high energy $E = 80$ MeV, at which the angular anisotropy $a = W(0°)/W(90°) - 1$ is still noticeably nonzero: the calculated value $a = 0.078$ is close to the experimental data for this region. In this case, the fission cross section $\sigma_f = 1793.1$ mb consists of about 80% of the isotropic component σ_f^{DPE} and only of 20% of the anisotropic component σ_f^C. According to our calculations, contributions to σ_f^C exceeding 1 mb come from 22 isotopes; 8 isotopes, ^{238}Np, ^{236}U, ^{235}U, ^{233}U, ^{232}U, ^{231}U, ^{230}U, and ^{234}Pa, give 80% of the cross section σ_f^C; and among these isotope, the largest contribution of 25% comes from the ^{230}U isotope. It is remarkable that this isotope alone gives the angular anisotropy $a = 0.024$, which constitutes 31% of the total value

$a = 0.078$ caused by all fissioning nuclei. A similar inclusion of only the eight isotopes listed above gives $a = 0.061$, which is 78% of the total value.

Since numerous isotopes with different Z and N values and different excitation energies contribute to the angular anisotropy of fission fragments, the used J_{eff} value is a certain average over the effective moments of inertia of fissioning nuclei. The same concerns the other parameters. The successful description of the angular anisotropy in the range from 0.4 to 160 MeV (see Fig. 1) with the minimum number of "averaged" parameters indicates that both the proposed method and the TALYS program are highly adequate. In particular, the calculation certainly indicates that a decrease in angular anisotropy above 30 MeV is due to an increase in the pre-equilibrium contributions to the reaction cross section. However, the energy ranges where the description does not reproduce the experimental data require a more detailed study. One of these ranges is the range above 100 MeV, where the calculations significantly underestimate the fission cross section possibly because of the overestimation of pre-equilibrium contributions. If this underestimation is confirmed and corrected, predictions for the angular anisotropy will also possibly increase, so that the experimental value $a = 0.072 \pm 0.011$ at $E = 95.8$ MeV, which currently seems overestimated, will be on the calculated curve. Attention should also be paid to the ranges of 15–20 and 1–4 MeV, where systematic, although different, discrepancies are observed between the calculated and measured quantities. At these relatively low energies, the number of fissioning isotopes determining the angular anisotropy of fission fragments is small and it is possibly necessary to take into account the dependence of the effective moment of inertia and other parameters on Z and N. Finally, of special interest is the range below 1 MeV, where the simplified model indicates two possible descriptions of the existing data on the angular anisotropy involving low and high K values. An increase in the accuracy of measurements of the angular anisotropy at 0.3–0.4 MeV will possibly allow the choice between these variants.

To summarize, the anisotropy of angular distributions of fragments from the fission of ^{237}Np nuclei induced by low- and intermediate-energy neutrons has been measured. A method for calculating these angular distributions has been developed using the TALYS program. The test of this method on the data obtained for the ^{237}Np target nucleus has indicated that it can be used to obtain new information on reactions at intermediate energies and on the fission process. In particular, the developed model makes it possible to determine contributions of individual isotopes to the observed angular anisotropy of fission fragments. The characteristics of transition states for the ^{238}Np nucleus have also been estimated.

ACKNOWLEDGMENTS

We are grateful to E.M. Ivanov and the staff of the Accelerator Department, Petersburg Nuclear Physics Institute, for their permanent friendly assistance and smooth operation of the synchrocyclotron during the experiment and to T.E. Kuz'mina (Khlopin Radium Institute, St. Petersburg, Russia) for cooperation in the preparation of high-quality actinide targets.

FUNDING

This work was supported in part by the Russian Foundation for Basic Research (project no. 18-02-00571).

REFERENCES

1. A. S. Vorobyev, A. M. Gagarski, O. A. Shcherbakov, L. A. Vaishnene, and A. L. Barabanov, JETP Lett. **102**, 203 (2015).
2. A. S. Vorobyev, A. M. Gagarski, O. A. Shcherbakov, L. A. Vaishnene, and A. L. Barabanov, JETP Lett. **104**, 365 (2016).
3. A. S. Vorobyev, A. M. Gagarski, O. A. Shcherbakov, L. A. Vaishnene, and A. L. Barabanov, JETP Lett. **107**, 521 (2018).
4. A. S. Vorobyev, A. M. Gagarski, O. A. Shcherbakov, L. A. Vaishnene, and A. L. Barabanov, EPJ Web of Conf. **146**, 04011 (2017).
5. A. S. Vorobyev, A. M. Gagarski, O. A. Shcherbakov, L. A. Vaishnene, and A. L. Barabanov, Bull. Russ. Acad. Sci.: Phys. **82**, 1240 (2018).
6. N. K. Abrosimov, G. Z. Borukhovich, A. B. Laptev, V. V. Marchenkov, G. A. Petrov, O. A. Shcherbakov, Yu. V. Tuboltsev, and V. I. Yurchenko, Nucl. Instrum. Methods Phys. Res., Sect. A **242**, 121 (1985).
7. O. A. Shcherbakov, A. S. Vorobyev, and E. M. Ivanov, Phys. Part. Nucl. **49**, 81 (2018).
8. D. Tarrio, L. S. Leong, L. Audouin, et al. (The n_TOF Collab.), Nucl. Data Sheets **119**, 35 (2014).
9. E. Leal-Cidoncha, I. Duran, C. Paradela, et al. (The n_TOF Collab.), EPJ Web Conf. **111**, 10002 (2016).
10. V. Geppert-Kleinrath, F. Tovesson, J. S. Barrett, et al. (NIFFTE Collab.), Phys. Rev. C **99**, 064619 (2019).
11. I. V. Ryzhov, M. S. Onegin, G. A. Tutin, J. Blomgren, N. Olsson, A. V. Prokofiev, and P.-U. Renberg, Nucl. Phys. A **760**, 19 (2005).
12. J. E. Brolley, Jr. and W. C. Dickinson, Phys. Rev. **94**, 640 (1954).
13. J. E. Simmons and R. L. Henkel, Phys. Rev. **120**, 198 (1960).
14. R. B. Leachman and L. Blumberg, Phys. Rev. **137**, B814 (1965).
15. R. H. Iyer and M. L. Sagu, in *Proceedings of the Nuclear and Solid State Physics Symposium, Madurai, India, 1970,* Vol. 2, p. 57.
16. D. L. Shpak, B. I. Fursov, and G. N. Smirenkin, Sov. J. Nucl. Phys. **12**, 19 (1971).

17. Kh. D. Androsenko, G. G. Korolev, and D. L. Shpak, Vopr. At. Nauki Tekh., Ser.: Yad. Konst. **46** (2), 9 (1982).
18. S. Ouichaoui, S. Juhasz, M. Varnagy, and J. Csikai, Acta Phys. Hung. **64**, 209 (1988).
19. V. V. Zerkin and B. Pritychenko, Nucl. Instrum. Methods Phys. Res. **888**, 31 (2018). http://www.nndc.bnl.gov/exfor.
20. R. Vandenbosch and J. R. Huizenga, *Nuclear Fission* (Academic, New York, 1973).
21. R. Capote, M. Herman, P. Oblozinsky, et al. (RIPL-3 Collab.), Nucl. Data Sheets **110**, 3107 (2009).
22. A. J. Koning, S. Hilaire, and M. C. Duijvestijn, in *Proceedings of the International Conference on Nuclear Data for Science and Technology, Nice, France, 2007,* Ed. by O. Bersillon, F. Gunsing, E. Bauge, R. Jacqmin, and S. Leray (EDP Sciences, 2008), p. 211.
23. K. Blum, *Density Matrix Theory and Applications,* 3rd ed. (Springer, Berlin, Heidelberg, 2012), Chap. 4.
24. O. Shcherbakov, A. Donets, A. Evdokimov, A. Fomichev, T. Fukahori, A. Hasegawa, A. Laptev, V. Maslov, G. Petrov, S. Soloviev, Yu. Tuboltsev, and A. Vorobyev, J. Nucl. Sci. Tech. **39**, Suppl. 2, 230 (2002).
25. C. Paradela, L. Tassan-Got, L. Audouin, et al. (The n_TOF Collab.), Phys. Rev. C **82**, 034601 (2010).
26. M. Diakaki, D. Karadimos, R. Vlastou, et al. (The n_TOF Collab.), Phys. Rev. C **93**, 034614 (2016).

Translated by R. Tyapaev